LAWRENCE
LIVERMORE
NATIONAL
LABORATORY

LLNL-JRNL-416867

# Meson-Baryon Scattering Lengths from Mixed-Action Lattice QCD

S. Beane, W. Detmold, T. Luu, K. Orginos, A. Parreno, A. Torok, A. Walker-Loud

September 16, 2009

Physical Review D

## Disclaimer


UNH-09-03
JLAB-THY-09-x
ICCUB-09-217
ATHENA-PUB-09-x

# Meson-Baryon Scattering Lengths from Mixed-Action Lattice QCD

S.R. Beane,[1] W. Detmold,[2,3] T.C. Luu,[4] K. Orginos,[2,3]
A. Parreño,[5] A. Torok,[1] and A. Walker-Loud[2]

(NPLQCD Collaboration)

[1]*Department of Physics, University of New Hampshire, Durham, NH 03824-3568.*
[2]*Department of Physics, College of William and Mary, Williamsburg, VA 23187-8795.*
[3]*Jefferson Laboratory, 12000 Jefferson Avenue, Newport News, VA 23606.*
[4]*N Division, Lawrence Livermore National Laboratory, Livermore, CA 94551.*
[5]*Departament d'Estructura i Constituents de la Matèria and Institut de Ciències del Cosmos, Universitat de Barcelona, E–08028 Barcelona, Spain.*

## Abstract

The $\pi^+\Sigma^+$, $\pi^+\Xi^0$, $K^+p$, $K^+n$, $\overline{K}^0\Sigma^+$, and $\overline{K}^0\Xi^0$ scattering lengths are calculated in mixed-action Lattice QCD with domain-wall valence quarks on the asqtad-improved coarse MILC configurations at four light-quark masses, and at two light-quark masses on the fine MILC configurations. Heavy Baryon Chiral Perturbation Theory with two and three flavors of light quarks is used to perform the chiral extrapolations. We find no convergence for the kaon-baryon processes in the three-flavor chiral expansion. Using the two-flavor chiral expansion, we find $a_{\pi^+\Sigma^+} = -0.197 \pm 0.017$ fm, and $a_{\pi^+\Xi^0} = -0.098 \pm 0.017$ fm, where the comprehensive error includes statistical and systematic uncertainties.

## I. INTRODUCTION

Lattice QCD calculations of meson-meson interactions have yielded predictions for physical scattering lengths at the few percent level [1–3]. Several reasons underlie this striking accuracy. Firstly, at the level of the lattice calculation, Euclidean-space correlation functions involving pseudoscalar mesons have signals that do not degrade, or only slowly degrade with time, and therefore, highly accurate fits of both single- and multi-meson properties are possible with currently available supercomputer resources. Indeed recent calculations have been performed with up to twelve mesons interacting on a lattice [4, 5] with no appreciable degradation of the signal with time. Secondly, and perhaps more importantly, QCD correlation functions with Goldstone bosons on external lines are subject to powerful chiral symmetry constraints which play an essential role in extrapolating the lattice data to the physical quark masses, as well as to the infinite volume and continuum limits. Chiral perturbation theory ($\chi$-PT) is the optimal method for implementing QCD constraints due to chiral symmetry and in essence provides an expansion of low-energy S-matrix elements in quark masses and powers of momentum [6].

By contrast with the purely mesonic sector, recent studies of baryon-baryon interactions, the paradigmatic nuclear physics process, have demonstrated the fundamental difficulty faced in making predictions for baryons and their interactions [7, 8]. Unlike the mesons, correlation functions involving baryons suffer an exponential degradation at large times [1], and therefore pose a fundamentally different kind of challenge in extracting signal from data [10]. Furthermore, while baryon interactions are constrained by QCD symmetries like chiral symmetry, the constraints are not nearly as powerful as when there is at least one pion or kaon in the initial or final state. For instance, there is no expectation that the baryon-baryon scattering lengths vanish in the chiral limit as they do in the purely mesonic sector. Moreover, in nucleon-nucleon scattering, the s-wave interactions are enhanced due to proximity to a non-trivial ultraviolet fixed point of the renormalization group, which drives the scattering lengths to infinity, thus rendering the effective field theory description of the interaction highly non-perturbative [11].

Given the contrast in difficulty between the purely mesonic and purely baryonic sectors described above, it is clearly of great interest to perform a lattice QCD investigation of the simplest scattering process involving at least one baryon: meson-baryon scattering. While pion-nucleon scattering is the best studied process, both theoretically and experimentally, its determination on the lattice involves so-called annihilation diagrams, which are very expensive and are only presently being studied in a few simple cases [12]. Combining the lowest-lying $SU(3)$ meson and baryon octets, one can form six meson-baryon elastic scattering processes that do not involve annihilation diagrams. Four of these involve kaons and therefore are, in principle, amenable to an $SU(3)$ heavy-baryon $\chi$-PT (HB$\chi$-PT) analysis [13] for extrapolation. The remaining two processes involve pions interacting with hyperons and therefore can be analyzed in conjunction with the kaon processes in $SU(3)$ HB$\chi$-PT, or independently using $SU(2)$ HB$\chi$-PT.

Meson-baryon scattering has been developed to several non-trivial orders in the $SU(3)$ HB$\chi$-PT expansion in Refs. [14, 15], extending earlier work on kaon-nucleon scattering

[1] A recent high-statistics study of baryon correlation functions on anisotropic clover lattices has found that the exponential decay with time of the signal occurs only *asymptotically* in time, and therefore the signal/noise problem in baryon correlation functions is not nearly as severe as previously thought [9].

in Ref. [16]. A very-recent paper [17] has reconsidered the $SU(3)$ HB$\chi$-PT results using a different regularization scheme, and also derived results for pion-hyperon scattering in the $SU(2)$ HB$\chi$-PT expansion. As all of these works make clear, given the paucity of experimental data, it is very difficulty to assess the convergence of the chiral expansion in the three-flavor case, and there is no experimental data which would allow one to consider pion-hyperon scattering separately in the two-flavor expansion. A lattice calculation of meson-baryon scattering analyzed using $\chi$-PT is therefore useful not only in making predictions for low-energy scattering at the physical point, but also for assessing the convergence of the chiral expansion for a range of quark masses at which present-day lattice calculations are being performed.

Meson-baryon scattering is also of interest for several indirect reasons. The kaon-nucleon interactions are important for the description of kaon condensation in the interior of neutron stars [18], and meson-baryon interactions are essential input in determining the final-state interactions of various decays that are interesting for standard-model phenomenology (See Ref. [19] for an example.). Finally, in determining baryon excited states on the lattice, it is clear that the energy levels that map to meson-baryon scattering on the lattice must be fully understood before any progress can be made regarding single-particle excitations.

The experimental input to existing $\chi$-PT analyses of meson-baryon scattering is extensively discussed in Refs. [14–17]. Threshold pion-nucleon scattering information is taken from experiments with pionic hydrogen and deuterium [20, 21], and the kaon-nucleon scattering lengths are taken from model-dependent extractions from kaon-nucleon scattering data [22]. There is essentially no experimental information available on the pion-hyperon and kaon-hyperon scattering lengths. There have been two quenched lattice QCD studies of meson-baryon scattering parameters: the pioneering work of Ref. [23] calculated pion-nucleon and kaon-nucleon scattering lengths at heavy pion masses without any serious attempt to extrapolate to the physical point, and Ref. [24] calculated the $I = 1$ $KN$ scattering length and found a result consistent with the current algebra prediction.

In this work we calculate the lowest-lying energy levels for the six meson-baryon processes that have no annihilation diagrams: $\pi^+\Sigma^+$, $\pi^+\Xi^0$, $K^+p$, $K^+n$, $\overline{K}^0\Sigma^+$, and $\overline{K}^0\Xi^0$ in a mixed-action Lattice QCD calculation with domain-wall valence quarks on the asqtad-improved coarse MILC configurations with $b \sim 0.125$ fm at four light-quark masses ($m_\pi \sim 291$, 352, 491 and 591 MeV), and at two light quark masses ($m_\pi \sim 320$ and 441 MeV) on the fine MILC configurations with $b \sim 0.09$ fm, with substantially less statistics on the fine ensembles. We extract the s-wave scattering lengths from the two-particle energies, and we analyze the six processes using $SU(3)$ HB$\chi$-PT. We find a rather conclusive lack of convergence in the three-flavor chiral expansion. We then consider $\pi^+\Sigma^+$ and $\pi^+\Xi^0$ using $SU(2)$ HB$\chi$-PT and we find that we are able to make reliable predictions of the scattering lengths at the physical point. We find

$$a_{\pi^+\Sigma^+} = -0.197 \pm 0.017 \text{ fm} ; \quad (1)$$

$$a_{\pi^+\Xi^0} = -0.098 \pm 0.017 \text{ fm} , \quad (2)$$

where the errors encompass statistical and systematic uncertainties. The leading order $\chi$-PT (current algebra) predictions for the scattering lengths are given by [25]:

$$a_{\pi^+\Sigma^+} = -0.2294 \text{ fm} ; \quad (3)$$

$$a_{\pi^+\Xi^0} = -0.1158 \text{ fm} . \quad (4)$$

| Particles | Isospin | Quark Content |
|---|---|---|
| $\pi^+\Sigma^+$ | 2 | $uuu\bar{d}s$ |
| $\pi^+\Xi^0$ | 3/2 | $uu\bar{d}ss$ |
| $K^+p$ | 1 | $uuud\bar{s}$ |
| $K^+n$ | 0 *and* 1 | $uudd\bar{s}$ |
| $\overline{K}^0\Sigma^+$ | 3/2 | $uu\bar{d}ss$ |
| $\overline{K}^0\Xi^0$ | 1 | $u\bar{d}sss$ |

TABLE I: Particle content, isospin and valence quark structure of the meson-baryon states calculated in this work. As is clear from the valence quark content, these meson-baryon states have no annihilation diagrams.

Ultimately, either the chiral extrapolation should be performed after a continuum limit has been taken, or one should use the mixed-action extension of HB$\chi$-PT to perform the chiral extrapolations [26, 27]. However, our results on the finer lattice spacing are statistics limited and therefore not yet sufficiently accurate to make this a useful exercise. Further, the explicit extrapolation formulae for the meson-baryon scattering lengths have not yet been determined in mixed-action $\chi$-PT. Despite these limitations, we expect the corrections from finite lattice spacing to be small for two principle reasons. First, the meson-baryon scattering lengths are protected by chiral symmetry and therefore the (approximate) chiral symmetry of the domain wall valence fermions used in this work protects the scattering lengths from additive renormalization, which can be explicitly seen in the construction of the mixed-action baryon Lagrangian in Ref. [27]. In fact, as can be shown, the mixed-action corrections do not appear until next-to-next-to leading order in the chiral expansion of the meson-baryon scattering lengths. Second, our previous experience with this mixed-action lattice QCD program leads us to expect that discretization effects will be well encompassed within the overall uncertainties we quote. In our precise calculation of meson-meson scattering, the predicted mixed-action corrections [28, 29] were smaller than the uncertainties on a given ensemble [1, 3].

This paper is organized as follows. In section II we isolate the six meson-baryon processes that have no annihilation diagrams and which are calculated in this work. We briefly review the standard Lüscher method for extracting the scattering amplitude from two-particle energy levels in a finite volume in section III. Particulars regarding the mixed-action lattice calculation and fitting methods are provided in section IV. Additional details can be found in Ref. [30]. In section V we consider chiral extrapolations of the lattice data using $SU(3)$ HB$\chi$-PT, and in section VI we analyze the pion-hyperon lattice data using $SU(2)$ HB$\chi$-PT. Finally, we conclude in section VII.

## II. MESON-BARYON SCATTERING PROCESSES

It is a straightforward exercise to construct the six elastic scattering channels involving the lowest-lying octet mesons and baryons that do not have annihilation diagrams, and to determine their isospin. The particle content, isospin, and valence quark content of these meson-baryon states are shown in Table I. We adopt the notation of Ref. [14], denoting the threshold T-matrix in the isospin basis as $T^{(I)}_{\phi B}$, where $I$ is the isospin of the meson-baryon

combination, $\phi$ is the meson, and $B$ is the baryon. The six elastic meson-baryon scattering processes that we consider are then in correspondence with the isospin amplitudes according to

$$\begin{aligned} T_{\pi^+\Sigma^+} &= T^{(2)}_{\pi\Sigma} \; ; \qquad T_{\pi^+\Xi^0} = T^{(3/2)}_{\pi\Xi} \; ; \\ T_{K^+p} &= T^{(1)}_{KN} \; ; \qquad T_{K^+n} = \frac{1}{2}(T^{(1)}_{KN} + T^{(0)}_{KN}) \; ; \\ T_{\overline{K}^0\Sigma^+} &= T^{(3/2)}_{K\Sigma} \; ; \qquad T_{\overline{K}^0\Xi^0} = T^{(1)}_{K\Xi} \; . \end{aligned} \tag{5}$$

These threshold T-matrices are related to the scattering lengths $a_{\phi B}$ through:

$$T_{\phi B} = 4\pi \left(1 + \frac{m_\phi}{m_B}\right) a_{\phi B} \; , \tag{6}$$

where $m_\phi$ is the meson mass and $m_B$ is the baryon mass.

## III. FINITE-VOLUME CALCULATION OF SCATTERING AMPLITUDES

The s-wave scattering amplitude for two particles below inelastic thresholds can be determined using Lüscher's method [31], which entails a measurement of one or more energy levels of the two-particle system in a finite volume. For two particles with masses $m_\phi$ and $m_B$ in an s-wave, with zero total three momentum, and in a finite volume, the difference between the energy levels and those of two non-interacting particles can be related to the inverse scattering amplitude via the eigenvalue equation [31]

$$p \cot \delta(p) \; = \; \frac{1}{\pi L} \, \mathbf{S} \left( \frac{pL}{2\pi} \right) \quad , \tag{7}$$

where $\delta(p)$ is the elastic-scattering phase shift, and the regulated three-dimensional sum is

$$\mathbf{S}\,(\,\eta\,) \; \equiv \; \sum_{\mathbf{j}}^{|\mathbf{j}|<\Lambda} \frac{1}{|\mathbf{j}|^2 - \eta^2} \; - \; 4\pi\Lambda \quad . \tag{8}$$

The sum in eq. (8) is over all triplets of integers $\mathbf{j}$ such that $|\mathbf{j}| < \Lambda$ and the limit $\Lambda \to \infty$ is implicit [32]. This definition is equivalent to the analytic continuation of zeta-functions presented by Lüscher [31]. In eq. (7), $L$ is the length of the spatial dimension in a cubically-symmetric lattice. The energy eigenvalue $E_n$ and its deviation from the sum of the rest masses of the particle, $\Delta E_n$, are related to the center-of-mass momentum $p_n$, a solution of eq. (7), by

$$\begin{aligned} \Delta E_n \; &\equiv \; E_n \; - \; m_\phi \; - \; m_B \; = \; \sqrt{\; p_n^2 \; + \; m_\phi^2 \;} \; + \; \sqrt{\; p_n^2 \; + \; m_B^2 \;} \; - \; m_\phi \; - \; m_B \\ &= \; \frac{p_n^2}{2\mu_{\phi B}} \; + \; \ldots \quad , \end{aligned} \tag{9}$$

where $\mu_{\phi B}$ is the reduced mass of the meson-baryon system. In the absence of interactions between the particles, $|p \cot \delta| = \infty$, and the energy levels occur at momenta $\mathbf{p} = 2\pi\mathbf{j}/L$,

corresponding to single-particle modes in a cubic cavity with periodic boundary conditions. Expanding eq. (7) about zero momenta, $p \sim 0$, one obtains the familiar relation [2]

$$\Delta E_0 \;=\; -\frac{2\pi a}{\mu_{\phi B} L^3}\left[\; 1 \;+\; c_1 \frac{a}{L} \;+\; c_2 \left(\frac{a}{L}\right)^2 \;\right] \;+\; \mathcal{O}\left(\frac{1}{L^6}\right) \quad , \tag{10}$$

with

$$c_1 \;=\; \frac{1}{\pi} \sum_{\mathbf{j}\neq\mathbf{0}}^{|\mathbf{j}|<\Lambda} \frac{1}{|\mathbf{j}|^2} \;-\; 4\Lambda \;\;=\; -2.837297 \quad , \quad c_2 \;=\; c_1^2 \;-\; \frac{1}{\pi^2} \sum_{\mathbf{j}\neq\mathbf{0}} \frac{1}{|\mathbf{j}|^4} \;\;=\; 6.375183 \;\; , \tag{11}$$

and $a$ is the scattering length, defined by

$$a \;=\; \lim_{p\to 0} \frac{\tan\delta(p)}{p} \; . \tag{12}$$

As the finite-volume lattice calculation cannot achieve $p = 0$ (except in the absence of interactions), in quoting a lattice value for the scattering length extracted from the ground-state energy level, it is important to determine the error associated with higher-order range corrections.

## IV. LATTICE CALCULATION AND DATA ANALYSIS

In calculating the meson-baryon scattering lengths, the mixed-action lattice QCD scheme was used in which domain-wall quark [33–37] propagators are generated from a smeared source on $n_f = 2 + 1$ asqtad-improved [38, 39] rooted staggered sea quarks [40]. To improve the chiral symmetry properties of the domain-wall quarks, hypercubic-smearing (HYP-smearing) [41–43] was used in the gauge links of the valence-quark action. In the sea-quark sector, there has been significant debate regarding the validity of taking the fourth root of the staggered fermion determinant at finite lattice spacing [44–57]. While there is no proof, there are arguments to suggest that taking the fourth root of the fermion determinant recovers the contribution from a single Dirac fermion. The results of this paper assume that the fourth-root trick recovers the correct continuum limit of QCD.

The present calculations were performed predominantly with the coarse MILC lattices with a lattice spacing of $b \sim 0.125$ fm, and a spatial extent of $L \sim 2.5$ fm. On these configurations, the strange quark was held fixed near its physical value while the degenerate light quarks were varied over a range of masses; see Table II and Ref. [30] for details. Results were also obtained on a coarse MILC ensemble with a spatial extent of $L \sim 3.5$ fm. However, this data is statistics limited. In addition, calculations were performed on two fine MILC ensembles at $L \sim 2.5$ fm with $b \sim 0.09$ fm. On the coarse MILC lattices, Dirichlet boundary conditions were implemented to reduce the original time extent of 64 down to 32 and thus save a nominal factor of two in computational time. While this procedure leads to minimal degradation of a nucleon signal, it does limit the number of time slices available for

[2] In order to be consistent with the meson-baryon literature, we have chosen to use the "particle physics" definition of the scattering length, as opposed to the "nuclear physics" definition, which is opposite in sign.

| Ensemble | $bm_l$ | $bm_s$ | $bm_l^{dwf}$ | $bm_s^{dwf}$ | $10^3 \times bm_{res}$ [a] | # of propagators |
|---|---|---|---|---|---|---|
| (*i*) 2064f21b676m007m050 | 0.007 | 0.050 | 0.0081 | 0.081 | $1.604 \pm 0.038$ | $1039 \times 24$ |
| (*ii*) 2064f21b676m010m050 | 0.010 | 0.050 | 0.0138 | 0.081 | $1.552 \pm 0.027$ | $769 \times 24$ |
| (*iii*) 2064f21b679m020m050 | 0.020 | 0.050 | 0.0313 | 0.081 | $1.239 \pm 0.028$ | $486 \times 24$ |
| (*iv*) 2064f21b681m030m050 | 0.030 | 0.050 | 0.0478 | 0.081 | $0.982 \pm 0.030$ | $564 \times 24$ |
| (*v*) 2864f21b676m010m050 | 0.010 | 0.050 | 0.0138 | 0.081 | $1.552 \pm 0.027$ | $128 \times 8$ |
| (*vi*) 2896f21b709m0062m031 | 0.0062 | 0.031 | 0.0080 | 0.0423 | $0.380 \pm 0.006$ | $1001 \times 8$ |
| (*vii*) 2896f21b709m0124m031 | 0.0124 | 0.031 | 0.0080 | 0.0423 | $0.380 \pm 0.006$ | $513 \times 3$ |

[a]Computed by the LHP collaboration for the coarse ensembles.

TABLE II: The parameters of the MILC gauge configurations and domain-wall propagators used in this work. The subscript $l$ denotes light quark (up and down), and $s$ denotes the strange quark. The superscript $dwf$ denotes the bare-quark mass for the domain-wall fermion propagator calculation. The last column is the number of configurations times the number of sources per configuration. Ensembles (*i*)-(*iv*) have $L \sim 2.5$ fm and $b \sim 0.125$ fm; Ensemble (*v*) has $L \sim 3.5$ fm and $b \sim 0.125$ fm; Ensembles (*vi*),(*vii*) have $L \sim 2.5$ fm and $b \sim 0.09$ fm.

fitting meson properties. By contrast, on the fine MILC ensembles, anti-periodic boundary conditions were implemented and all time slices are available.

The correlation function that projects onto the zero momentum state for the meson-baryon system is:

$$C_{\phi B}(t) = \sum_{\mathbf{x},\mathbf{y}} \langle \phi^\dagger(t,\mathbf{x}) \overline{B}(t,\mathbf{y}) \phi(0,\mathbf{0}) B(0,\mathbf{0}) \rangle \ . \tag{13}$$

For instance, in the case of $K^+p$, the interpolating operators for the $K^+$ and the proton are:

$$\begin{aligned} \phi(t,\mathbf{x}) &= K^+(t,\mathbf{x}) = \overline{s}(t,\mathbf{x})\gamma_5 u(t,\mathbf{x}) \ ; \\ B_i(t,\mathbf{x}) &= p_i(t,\mathbf{x}) = \epsilon_{abc} u_i^a(t,\mathbf{x}) \left( u^{b\mathrm{T}}(t,\mathbf{x}) C\gamma_5 d^c(t,\mathbf{x}) \right) \ . \end{aligned} \tag{14}$$

The masses of the mesons and baryons are extracted using the assumed form of the large-time behavior of the single particle correlators as a function of time. As $t \to \infty$, the ground state dominates, however, the contribution from fluctuations of the correlator due to the dynamical quarks increases with respect to the ground state. The fluctuations with the same quantum numbers as the correlator appear as noise in the signal. The single particle states behave as:

$$C_{\phi,B}(t) \ \to \ \mathcal{A} \ e^{-m_{\phi,B} \ t} \ . \tag{15}$$

In relatively large lattice volumes the energy difference between the interacting and non-interacting meson-baryon states is a small fraction of the total energy, which is dominated by the masses of the mesons and baryons [1]. In order to extract this energy difference the ratio of correlation functions, $G_{\phi B}(t)$, is formed:

$$G_{\phi B}(t) \equiv \frac{C_{\phi B}(t)}{C_\phi(t) C_B(t)} \ \to \ \sum_{n=0}^{\infty} \ \mathcal{A}_n \ e^{-\Delta E_n \ t} \ . \tag{16}$$

Once $\Delta E$ is obtained, the scattering length can be calculated using eqs. (7) and (9), or, if $a << L$, from eq. (10). For the meson-baryon scattering lengths calculated in this work, the difference between the exact and perturbative eigen-equations is negligible.

We use a variety of fitting methods, including standard chi-square minimization fits to one and two exponentials. Generalized effective energy plots are particularly useful for analyzing the lattice data and for estimating systematic errors [9]. These plots are constructed by taking the ratio of the correlators at times $t$, and $t + n_J$ (where $n_J$ is an integer):

$$m^{\rm eff}_{\phi,B} = \frac{1}{n_J}\log\left(\frac{C_{\phi,B}(t)}{C_{\phi,B}(t+n_J)}\right), \qquad \Delta E^{\rm eff}_{\phi B} = \frac{1}{n_J}\log\left(\frac{G_{\phi B}(t)}{G_{\phi B}(t+n_J)}\right) . \tag{17}$$

With $n_J = 1$ one recovers the standard effective mass and energy plots. Generalized effective masses form a system of linear equations for each $n_J$ over the time interval where the data is fit. For instance, if the interval is given by $\Delta t = t_2 - t_1$, then there is one equation for $m^{\rm eff}$ at each $t_n$ within $\Delta t$ for $1 \leq n_J \leq \Delta t$ at each $t + n_J \leq t_2$. The equations can be solved for $m^{\rm eff}$ by casting them into the form of the so-called normal equation [58]. Since each $n_J$ constitutes a different effective mass plot, the number of degrees of freedom is increased significantly. This method provides a fitting routine that is faster than standard least-squares fitting. Additional details regarding the utility of generalized effective mass and energy plots can be found in Ref. [59].

Our interpolating-operator at the source is constructed from gauge-invariantly-smeared quark field operators, while at the sink, the interpolating operator is constructed from either local quark field operators, or from the same smeared quark field operators used at the source, leading to two sets of correlation functions. For brevity, we refer to the two sets of correlation functions that result from these source and sink operators as *smeared-point* (SP) and *smeared-smeared* (SS) correlation functions, respectively. By forming a linear combination of the SP and SS correlation functions, $C^{(\rm SS)} - \alpha C^{(\rm SP)}$, we are able to remove the first excited state, thus gaining early time slices for fitting [59]. This effect is illustrated in Fig. 1, which is the effective $\Delta E_{\pi^+\Sigma^+}$ plot for coarse MILC ensemble (*ii*). We plot $C^{(\rm SS)}$, $C^{(\rm SP)}$ and $C^{(\rm SS)} - \alpha C^{(\rm SP)}$ with $\alpha$ tuned to remove the first excited state. All effective masses and energy splittings are plotted for coarse MILC ensemble (*ii*) in figs. 2 and 3.

All of the necessary quantities needed for extraction of the scattering lengths are contained in Table III. The sum of meson and baryon masses is also tabulated at each quark mass. Note that as $\pi^+\Xi^0$ and $\overline{K}^0\Sigma^+$ carry the same quantum numbers and $\pi^+\Xi^0$ is lower in energy, *a priori* we expect difficulties in extracting the $\overline{K}^0\Sigma^+$ energy level. One might expect that the $\pi^+\Xi^0$ state would be the lowest-lying energy level coupling to the $\overline{K}^0\Sigma^+$ interpolating operator. However, within statistical and systematic errors, we find distinct energy levels from the two interpolating operators consistent with coupling primarily to the interpolating operator color-singlet constituents. Nevertheless, one should keep in mind that this introduces a significant systematic in the lattice extractions of the $\overline{K}^0\Sigma^+$ scattering lengths. At the operational level, the appearance of the $\pi^+\Xi^0$ intermediate state in loop diagrams for the $\overline{K}^0\Sigma^+$ amplitude in HB$\chi$-PT generates an imaginary contribution to the scattering length.

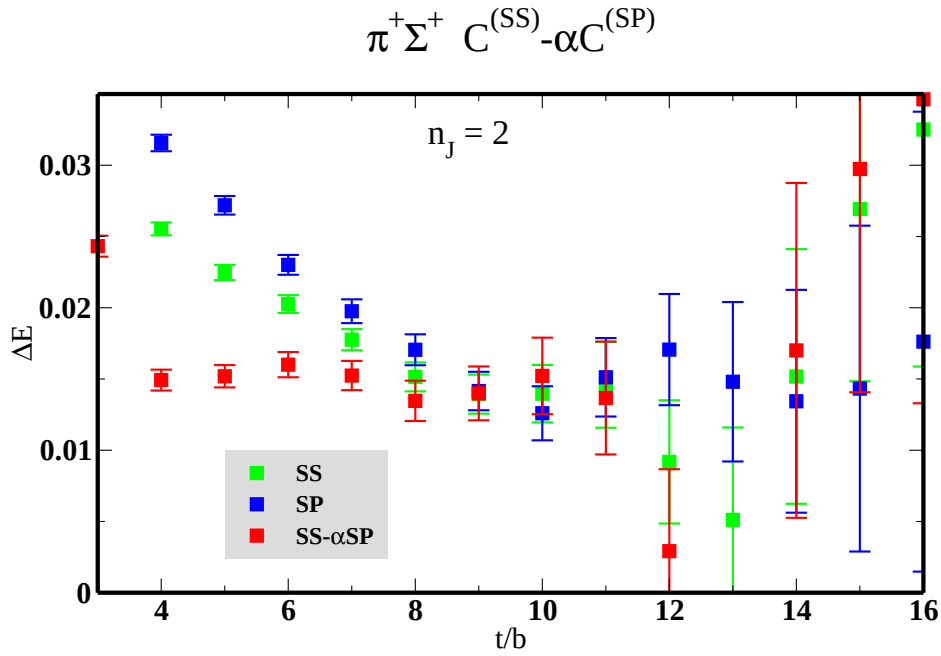


FIG. 1: Effective $\Delta E_{\pi^+\Sigma^+}$ plot for coarse MILC ensemble (*ii*) from correlation functions $C^{(\mathrm{SS})}$, $C^{(\mathrm{SP})}$ and $C^{(\mathrm{SS})} - \alpha C^{(\mathrm{SP})}$. By taking the linear combination with $\alpha$ tuned to remove the first excited state, earlier time slices are gained for fitting.

## V. SU(3) HB$\chi$PT EXTRAPOLATION

### A. Scattering Length Formulas

The scattering lengths of the six meson-baryon processes listed in eq. (5) are, to $\mathcal{O}(m_\pi^3)$ in $SU(3)$ HB$\chi$-PT [14, 15],

$$a_{\pi^+\Sigma^+} = \frac{1}{4\pi}\frac{m_\Sigma}{m_\pi + m_\Sigma}\left[ -\frac{2m_\pi}{f_\pi^2} + \frac{2m_\pi^2}{f_\pi^2}C_1 + \mathcal{Y}_{\pi^+\Sigma^+}(\mu) + 8h_{123}(\mu)\frac{m_\pi^3}{f_\pi^2}\right] ; \tag{18}$$

$$a_{\pi^+\Xi^0} = \frac{1}{4\pi}\frac{m_\Xi}{m_\pi + m_\Xi}\left[ -\frac{m_\pi}{f_\pi^2} + \frac{m_\pi^2}{f_\pi^2}C_{01} + \mathcal{Y}_{\pi^+\Xi^0}(\mu) + 8h_1(\mu)\frac{m_\pi^3}{f_\pi^2}\right] ; \tag{19}$$

$$a_{K^+p} = \frac{1}{4\pi}\frac{m_N}{m_K + m_N}\left[ -\frac{2m_K}{f_K^2} + \frac{2m_K^2}{f_K^2}C_1 + \mathcal{Y}_{K^+p}(\mu) + 8h_{123}(\mu)\frac{m_K^3}{f_K^2}\right] ; \tag{20}$$

$$a_{K^+n} = \frac{1}{4\pi}\frac{m_N}{m_K + m_N}\left[ -\frac{m_K}{f_K^2} + \frac{m_K^2}{f_K^2}C_{01} + \mathcal{Y}_{K^+n}(\mu) + 8h_1(\mu)\frac{m_K^3}{f_K^2}\right] ; \tag{21}$$

$$a_{\overline{K}^0\Sigma^+} = \frac{1}{4\pi}\frac{m_\Sigma}{m_K + m_\Sigma}\left[ -\frac{m_K}{f_K^2} + \frac{m_K^2}{f_K^2}C_{01} + \mathcal{Y}_{\overline{K}^0\Sigma^+}(\mu) + 8h_1(\mu)\frac{m_K^3}{f_K^2}\right] ; \tag{22}$$

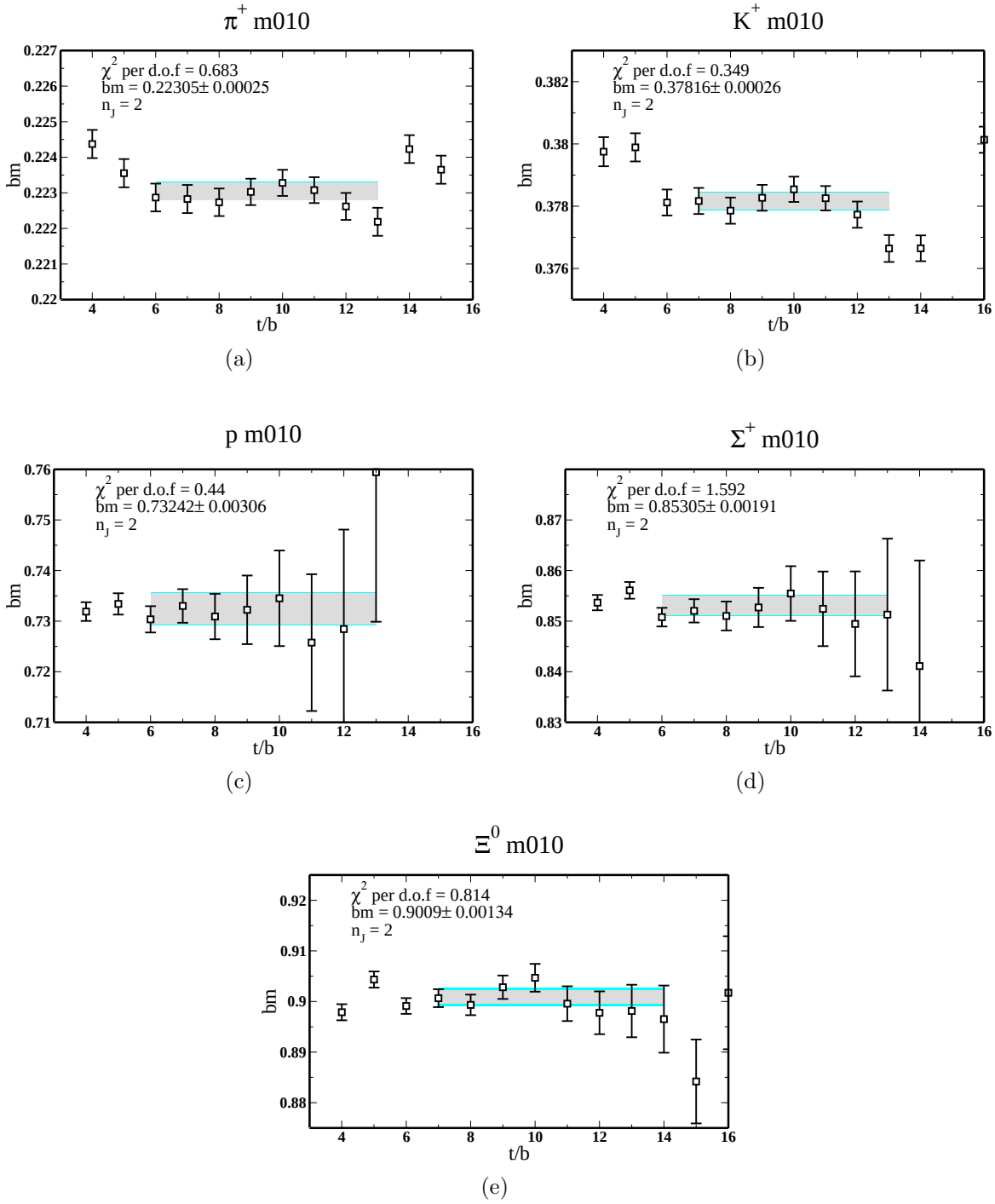


FIG. 2: Single particle effective mass plots for coarse MILC ensemble (*ii*). Here we choose $n_J = 2$, and the linear combination $C^{(\mathrm{SS})} - \alpha C^{(\mathrm{SP})}$ is plotted. The inner shaded bands are the jackknife errors of the fits to the effective masses, and the outer bands are the jackknife error and systematic error added in quadrature over the indicated window of time slices.

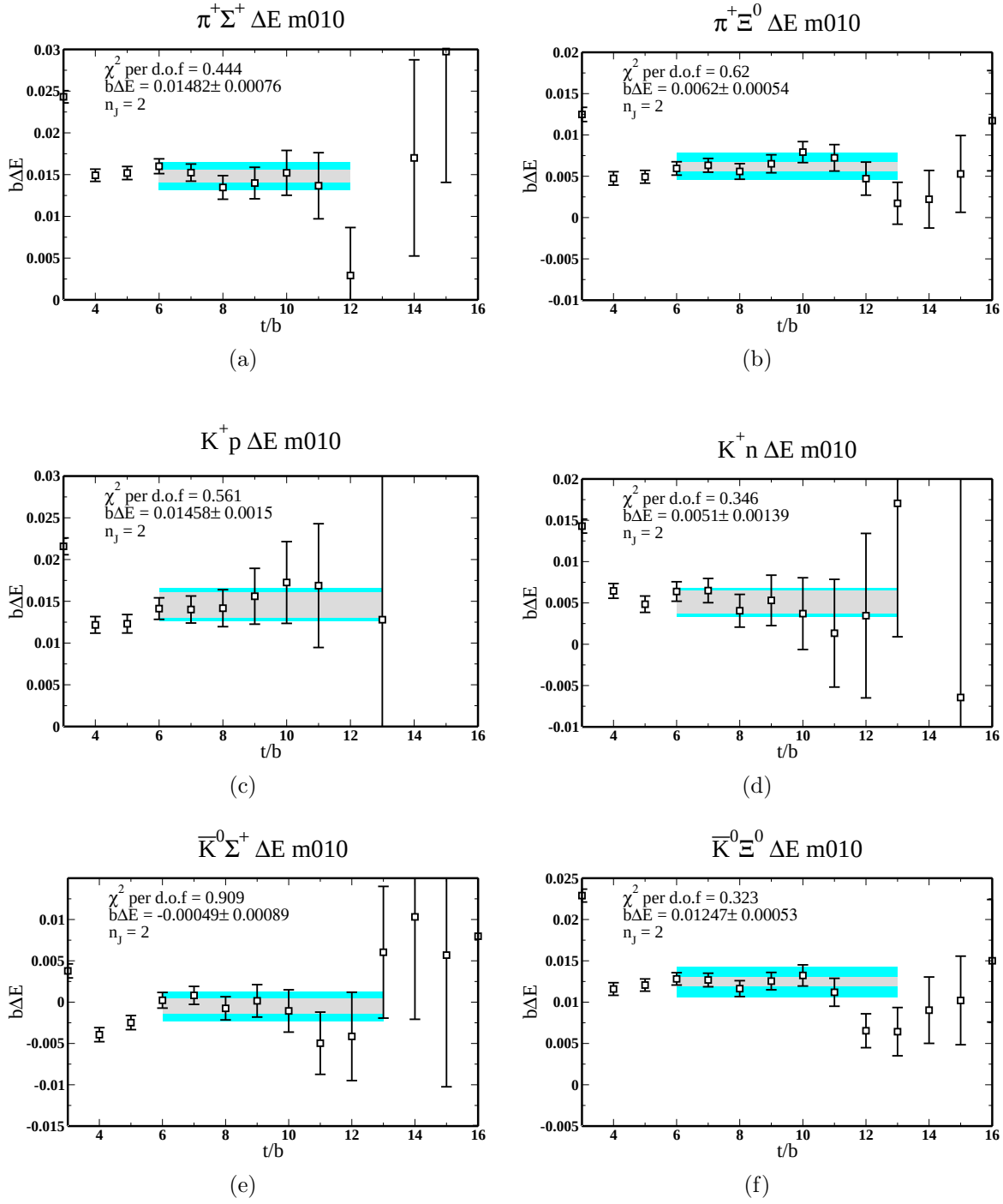


FIG. 3: Meson-baryon effective energy difference plots for coarse MILC ensemble (*ii*). Here we choose $n_J = 2$, and the linear combination $C^{(\mathrm{SS})} - \alpha C^{(\mathrm{SP})}$ is plotted. The inner shaded bands are the jackknife errors of the fits to the effective energy differences, and the outer bands are the jackknife error and systematic error added in quadrature over the indicated window of time slices.

| Quantity | m007 (*i*) | m010 (*ii*) | m020 (*iii*) | m030 (*iv*) |
|---|---|---|---|---|
| $m_\pi$ | 0.18384(31)(03) | 0.22305(25)(08) | 0.31031(38)(95) | 0.37513(44)(13) |
| $m_k$ | 0.36783(32)(42) | 0.37816(26)(11) | 0.40510(33)(37) | 0.43091(66)(16) |
| $m_p$ | 0.6978(61)(08) | 0.7324(31)(10) | 0.8069(22)(14) | 0.8741(16)(05) |
| $m_\Sigma$ | 0.8390(22)(03) | 0.8531(19)(08) | 0.8830(18)(17) | 0.9213(13)(03) |
| $m_\Xi$ | 0.8872(13)(16) | 0.9009(13)(10) | 0.9233(18)(04) | 0.9461(14)(08) |
| $f_\pi$ | 0.09257(16) | 0.09600(14) | 0.10208(14) | 0.10763(32) |
| $f_K$ | 0.10734(10) | 0.10781(18) | 0.10976(17) | 0.11253(31) |
| $\Delta E_{\pi\Sigma}$ | 0.0150(14)(08) | 0.0148(08)(13) | 0.0111(10)(08) | 0.0100(10)(11) |
| $\Delta E_{\pi\Xi}$ | 0.00646(64)(98) | 0.0062(05)(12) | 0.00431(68)(43) | 0.00421(76)(60) |
| $\Delta E_{Kp}$ | 0.0140(22)(30) | 0.0146(15)(13) | 0.0092(10)(51) | 0.0087(16)(16) |
| $\Delta E_{Kn}$ | 0.0057(18)(16) | 0.0051(14)(09) | 0.0036(09)(12) | 0.0028(10)(11) |
| $\Delta E_{K\Sigma}$ | -0.0023(11)(24) | -0.0005(09)(17) | 0.0019(08)(11) | 0.0005(14)(16) |
| $\Delta E_{K\Xi}$ | 0.0118(08)(13) | 0.0125(05)(14) | 0.0085(08)(31) | 0.0086(16)(16) |
| $a_{\pi\Sigma}$ | -2.12(16)(09) | -2.36(09)(15) | -2.30(15)(13) | -2.36(18)(19) |
| $a_{\pi\Xi}$ | -1.08(09)(14) | -1.19(09)(20) | -1.08(15)(09) | -1.20(18)(15) |
| $a_{Kp}$ | -2.80(32)(44) | -2.95(21)(19) | -2.3(0.2)(1.0) | -2.27(31)(32) |
| $a_{Kn}$ | -1.41(37)(34) | -1.33(30)(21) | -1.05(22)(30) | -0.89(27)(31) |
| $a_{K\Sigma}$ | 0.9(0.4)(1.1) | 0.17(31)(61) | -0.60(23)(34) | -0.16(51)(57) |
| $a_{K\Xi}$ | -2.62(13)(21) | -2.77(08)(23) | -2.18(15)(63) | -2.29(30)(32) |
| $m_\pi + m_p$ | 0.8817(61) | 0.9555(31) | 1.1172(23) | 1.2492(18) |
| $m_\pi + m_\Sigma$ | 1.0229(23) | 1.0761(20) | 1.1933(19) | 1.2964(15) |
| $m_\pi + m_\Xi$ | 1.0710(14) | 1.1240(14) | 1.2336(19) | 1.3212(16) |
| $m_K + m_p$ | 1.0657(61) | 1.1106(31) | 1.2119(23) | 1.3050(19) |
| $m_K + m_\Sigma$ | 1.2069(23) | 1.2312(20) | 1.2881(19) | 1.3522(16) |
| $m_K + m_\Xi$ | 1.2550(14) | 1.2791(15) | 1.3284(19) | 1.3770(17) |

TABLE III: Lattice physical quantities from the four coarse MILC ensembles which enter the analysis of the meson-baryon scattering lengths. The first error is statistical and the second error is systematic due to fitting. All quantities are in lattice units.

$$a_{\overline{K}^0\Xi^0} = \frac{1}{4\pi}\frac{m_\Xi}{m_K + m_\Xi}\left[ -\frac{2m_K}{f_K^2} + \frac{2m_K^2}{f_K^2}C_1 + \mathcal{Y}_{\overline{K}^0\Xi^0}(\mu) + 8h_{123}(\mu)\frac{m_K^3}{f_K^2}\right] , \tag{23}$$

where we have defined $C_{01} \equiv C_0 + C_1$ and $h_{123} \equiv h_1 - h_2 + h_3$, and the loop functions are given by:

$$\begin{aligned}\mathcal{Y}_{\pi^+\Sigma^+}(\mu) \;=\; & \frac{m_\pi^2}{2\pi^2 f_\pi^4}\Bigg\{ -m_\pi\left(\frac{3}{2} - 2\ln\frac{m_\pi}{\mu} - \ln\frac{m_K}{\mu}\right) \\ & -\sqrt{m_K^2 - m_\pi^2}\,\arccos\frac{m_\pi}{m_K} + \frac{\pi}{2}\left[3F^2 m_\pi - \frac{1}{3}D^2 m_\eta\right]\Bigg\} ;\end{aligned} \tag{24}$$

$$\mathcal{Y}_{\pi^+\Xi^0}(\mu) \;=\; \frac{m_\pi^2}{4\pi^2 f_\pi^4}\Bigg\{ -m_\pi\left(\frac{3}{2}-2\ln\frac{m_\pi}{\mu}-\ln\frac{m_K}{\mu}\right)-\sqrt{m_K^2-m_\pi^2}\left(\pi+\arccos\frac{m_\pi}{m_K}\right)$$
$$+\frac{\pi}{4}\left[3(D-F)^2 m_\pi-\frac{1}{3}(D+3F)^2 m_\eta\right]\Bigg\}\;; \tag{25}$$

$$\mathcal{Y}_{K^+p}(\mu) \;=\; \frac{m_K^2}{4\pi^2 f_K^4}\Bigg\{m_K\left(-3+2\ln\frac{m_\pi}{\mu}+\ln\frac{m_K}{\mu}+3\ln\frac{m_\eta}{\mu}\right)$$
$$+2\sqrt{m_K^2-m_\pi^2}\ln\frac{m_K+\sqrt{m_K^2-m_\pi^2}}{m_\pi}-3\sqrt{m_\eta^2-m_K^2}\arccos\frac{m_K}{m_\eta}$$
$$-\frac{\pi}{6}(D-3F)\left[2(D+F)\frac{m_\pi^2}{m_\eta+m_\pi}+(D+5F)m_\eta\right]\Bigg\}\;; \tag{26}$$

$$\mathcal{Y}_{K^+n}(\mu) \;=\; \frac{\mathcal{Y}_{K^+p}}{2}+\frac{3m_K^2}{8\pi^2 f_K^4}\Bigg\{m_K\left(\ln\frac{m_\pi}{\mu}-\ln\frac{m_K}{\mu}\right)+\sqrt{m_K^2-m_\pi^2}\ln\frac{m_K+\sqrt{m_K^2-m_\pi^2}}{m_\pi}$$
$$+\frac{\pi}{3}(D-3F)\left[(D+F)\frac{m_\pi^2}{m_\eta+m_\pi}+\frac{1}{6}(7D+3F)m_\eta\right]\Bigg\}\;; \tag{27}$$

$$\mathcal{Y}_{\overline{K}^0\Sigma^+}(\mu) \;=\; \frac{m_K^2}{8\pi^2 f_K^4}\Bigg\{-m_K\left(3+\ln\frac{m_\pi}{\mu}-4\ln\frac{m_K}{\mu}-3\ln\frac{m_\eta}{\mu}\right)$$
$$+\sqrt{m_K^2-m_\pi^2}\left(2i\,\pi-\ln\frac{m_K+\sqrt{m_K^2-m_\pi^2}}{m_\pi}\right)-3\sqrt{m_\eta^2-m_K^2}\arccos\frac{m_K}{m_\eta}$$
$$+\frac{4}{3}\pi D\left[-2F\frac{m_\pi^2}{m_\eta+m_\pi}+(D-2F)m_\eta\right]\Bigg\}\;; \tag{28}$$

$$\mathcal{Y}^{(1)}_{\overline{K}^0\Xi^0}(\mu) \;=\; \frac{m_K^2}{4\pi^2 f_K^4}\Bigg\{m_K\left(-3+2\ln\frac{m_\pi}{\mu}+\ln\frac{m_K}{\mu}+3\ln\frac{m_\eta}{\mu}\right)$$
$$+2\sqrt{m_K^2-m_\pi^2}\ln\frac{m_K+\sqrt{m_K^2-m_\pi^2}}{m_\pi}-3\sqrt{m_\eta^2-m_K^2}\arccos\frac{m_K}{m_\eta}$$
$$-\frac{\pi}{6}(D+3F)\left[2(D-F)\frac{m_\pi^2}{m_\eta+m_\pi}+(D-5F)m_\eta\right]\Bigg\}\;. \tag{29}$$

In what follows, we choose $\mu=\Lambda_\chi=4\pi f_\pi$ and evaluate $f_\pi$ at its lattice physical value [60], and we take $m_\eta$ from the Gell-Mann-Okubo formula. These choices modify the chiral expansion at $\mathcal{O}(m_\pi^4)$ and are therefore consistent to the order we are working. Note that the $\overline{K}^0\Sigma^+$ loop function contains an imaginary part associated with the real $\pi^+\Xi^0$ intermediate state. In the analysis that follows we consider only the real part of the $\overline{K}^0\Sigma^+$ scattering length. The first mixed-action modification to these HB$\chi$-PT extrapolation formulae would appear as corrections to these loop functions, $\mathcal{Y}_{\phi B}$, and the corresponding counterterms which absorb the scale dependence. Some of the mesons propagating in the loops would be of a mixed valence-sea type, and thus the corresponding meson masses appearing in these functions would be heavier by a known amount [61]. The precise form of the predicted corrections would require a computation of the scattering processes with mixed-action/partially quenched $\chi$-PT.

We choose our physical parameter set to be consistent with Ref. [17] (note that our decay constant convention differs by $\sqrt{2}$). We take $f_\pi = 130.7$ MeV, $m_\pi = 139.57$ MeV, $f_K = 159.8$ MeV, $m_K = 493.68$ MeV, $m_N = 938$ MeV, $m_\Sigma = 1192$ MeV and $m_\Xi = 1314$ MeV. We take the axial couplings $D$ and $F$ for coarse MILC ensembles (*ii*)-(*iv*) from the mixed-action calculation of Ref. [62], and we use extrapolation for coarse MILC ensemble (*i*).

### B. Extrapolation to the Physical Point

For purpose of fitting and visualization, it is useful to construct from the scattering lengths the functions $\Gamma^{(1,2)}$ which are polynomials in $m_\phi$. For the $\pi^+\Sigma^+$, $Kp$, and $\overline{K}^0\Xi^0$ processes one defines[3]

$$\Gamma^{(1)}_{LO} \equiv -\frac{2\pi a f_\phi^2}{m_\phi}\left(1+\frac{m_\phi}{m_B}\right) = 1 \ ; \tag{30}$$

$$\Gamma^{(1)}_{NLO} \equiv -\frac{2\pi a f_\phi^2}{m_\phi}\left(1+\frac{m_\phi}{m_B}\right) = 1 - C_1 m_\phi \ ; \tag{31}$$

$$\Gamma^{(1)}_{NNLO} \equiv -\frac{2\pi a f_\phi^2}{m_\phi}\left(1+\frac{m_\phi}{m_B}\right) + \frac{f_\phi^2}{2m_\phi}\mathcal{Y}_{\phi B}(\Lambda_\chi) = 1 - C_1 m_\phi - 4h_{123}(\Lambda_\chi)m_\phi^2 \ , \tag{32}$$

and for the $\pi^+\Xi^0$, $Kn$, and $\overline{K}^0\Sigma^+$ processes one defines

$$\Gamma^{(2)}_{LO} \equiv -\frac{4\pi a f_\phi^2}{m_\phi}\left(1+\frac{m_\phi}{m_B}\right) = 1 \ ; \tag{33}$$

$$\Gamma^{(2)}_{NLO} \equiv -\frac{4\pi a f_\phi^2}{m_\phi}\left(1+\frac{m_\phi}{m_B}\right) = 1 - C_{01} m_\phi \ ; \tag{34}$$

$$\Gamma^{(2)}_{NNLO} \equiv -\frac{4\pi a f_\phi^2}{m_\phi}\left(1+\frac{m_\phi}{m_B}\right) + \frac{f_\phi^2}{m_\phi}\mathcal{Y}_{\phi B}(\Lambda_\chi) = 1 - C_{01} m_\phi - 8h_1(\Lambda_\chi)m_\phi^2 \ . \tag{35}$$

Notice that the left-hand sides of these equations are given entirely in terms of lattice-determined quantities, all evaluated under Jackknife, whereas the right-hand side provides a convenient polynomial fitting function. Plots of $\Gamma_{NLO}$ formed from the lattice data (all ensembles listed in table II) versus the Goldstone masses are given in Figure 4. We see evidence in this plot that the fine and large-volume coarse data are statistically limited as compared to the coarse data. Therefore, we include only the coarse data in our fits. The fine data is, however, indicative that lattice-spacing effects are small.

In the three-flavor chiral expansion, we have an overdetermined system at both NLO and NNLO. While there are six observables, there are two Low Energy Constants (LECs) at NLO, $C_0$ and $C_{01}$, and two LECs at NNLO, $h_1$ and $h_{123}$. Fits of the LECs from each process

[3] Here we use the standard notation, LO = leading order, NLO = next-to-leading order and so on.

| Quantity | NLO fit each process | NNLO fit $\pi^+\Sigma^+$,$\pi^+\Xi^0$ |
|---|---|---|
| $C_1(\pi^+\Sigma^+)$ | 0.66(04)(11) GeV$^{-1}$ | 3.51(18)(25) GeV$^{-1}$ |
| $C_{01}(\pi^+\Xi^0)$ | 0.69(06)(22) GeV$^{-1}$ | 7.44(29)(69) GeV$^{-1}$ |
| $C_1(K^+p)$ | 0.44(09)(23) GeV$^{-1}$ | - |
| $C_{01}(K^+n)$ | 0.56(11)(27) GeV$^{-1}$ | - |
| $C_{01}(\overline{K}^0\Sigma^+)$ | 1.55(31)(57) GeV$^{-1}$ | - |
| $C_1(\overline{K}^0\Xi^0)$ | 0.50(06)(14) GeV$^{-1}$ | - |
| $h_1$ | - | -0.59(08)(14) GeV$^{-2}$ |
| $h_{123}$ | - | -0.42(10)(10) GeV$^{-2}$ |

TABLE IV: $SU(3)$ LECs fit from each process at NLO, and from $\pi^+\Sigma^+$, and $\pi^+\Xi^0$ at NNLO. The first error in parentheses is statistical, and the second is the statistical and systematic error added in quadrature.

at NLO are given in table IV and the corresponding values of the scattering lengths are given in table V. At NLO, the LECs are of natural size, and with the exception of $\overline{K}^0\Sigma^+$, provide a consistent extraction within errors. Correspondingly, the scattering lengths, again with the exception of $\overline{K}^0\Sigma^+$, appear to deviate perturbatively from the LO values. The perturbative behavior of the scattering lengths at NLO is evident from the plots of $\Gamma_{NLO}$ versus the Goldstone masses given in Figure 5. Clearly the deviations of the lattice data from unity are consistent with a perturbative expansion.

At NNLO the situation changes dramatically. This is clear from the plots of $\Gamma_{NNLO}$ versus the Goldstone masses given in Figure 5. The shift of the value of $\Gamma$ from NLO to NNLO is dependent on the renormalization scale $\mu$. With the choice $\mu = \Lambda_\chi$ one would expect this shift to be perturbative. However, this is not the case and therefore loop corrections are very large at the scale $\Lambda_\chi$. There are many strategies that one may take to fit the LECs in the overdetermined system. Here we fit the LECs to the $\pi^+\Sigma^+$ and $\pi^+\Xi^0$ data, and then use these LECs to predict the kaon processes. Therefore, in figure 5, only (a) and (b) are fits. The fit LECs are given in table IV. While the NNLO LECs $h_1$ and $h_{123}$ appear to be of natural size, the NLO LECs $C_0$ and $C_{01}$ are unnaturally large and therefore are countering the large loop effects. The extrapolated $\pi^+\Sigma^+$ and $\pi^+\Xi^0$ scattering lengths are given in table V and appear to be perturbative. Table V also gives the extrapolated kaon-baryon scattering lengths with the LECs determined from $\pi^+\Sigma^+$ and $\pi^+\Xi^0$ data. The resulting NNLO predictions deviate by at least 100% from the LO values. Other fitting strategies lead to this same conclusion: the kaon-baryon scattering lengths are unstable against chiral corrections in the three-flavor chiral expansion, over the range of light-quark masses that we consider.

## VI. SU(2) HB$\chi PT$ EXTRAPOLATION

Given the poor convergence seen in the three-flavor chiral expansion due to the large loop corrections, it is natural to consider the two-flavor theory with the strange quark integrated out. In this way, $\pi\Sigma$ and $\pi\Xi$ may be analyzed in an expansion in $m_\pi$ with no fear of corrections that scale as powers of $m_K$. The detailed matching of LECs between the three-

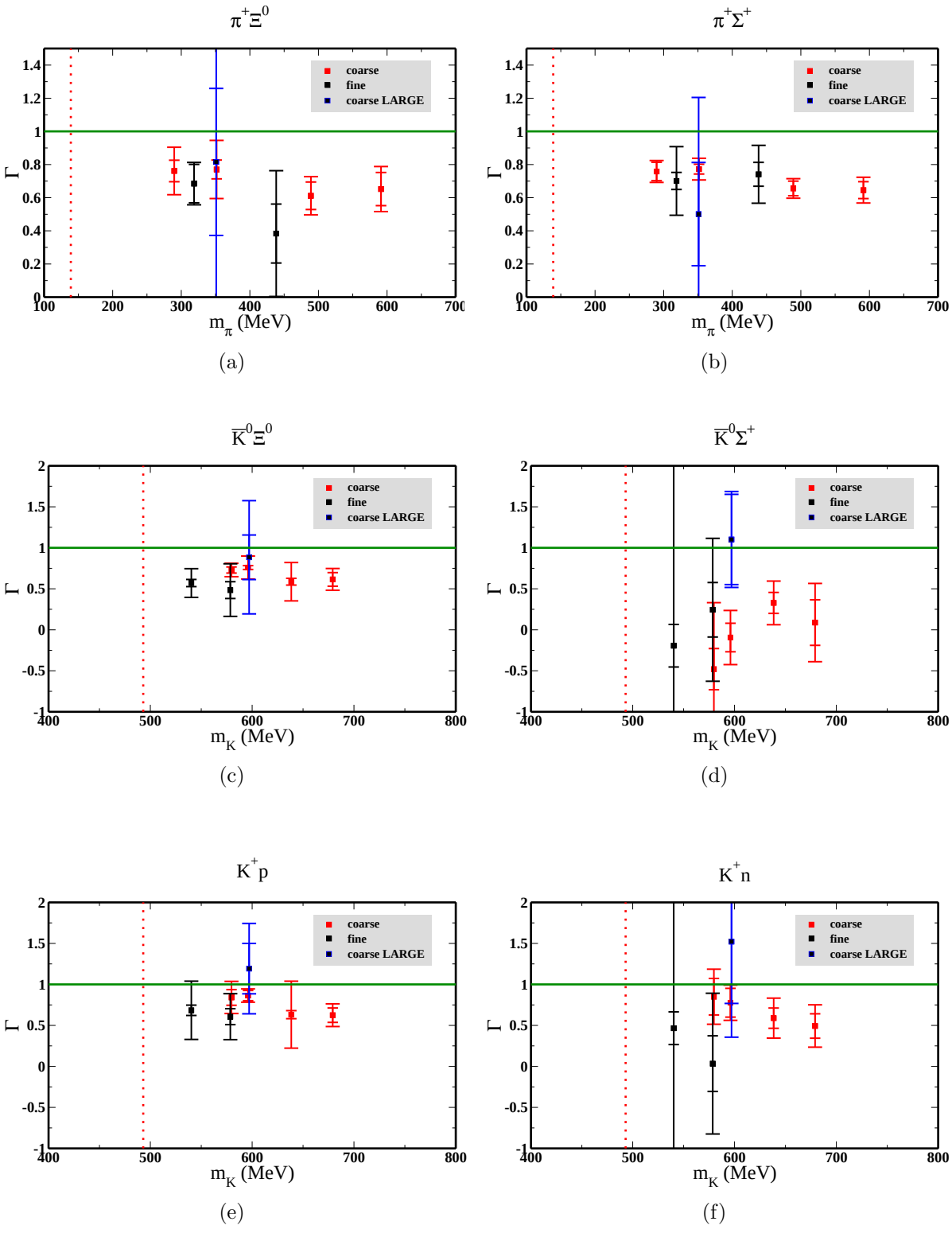


FIG. 4: Plots of $\Gamma_{NLO}$ versus the Goldstone masses for the six meson-baryon processes. All lattice data is included.

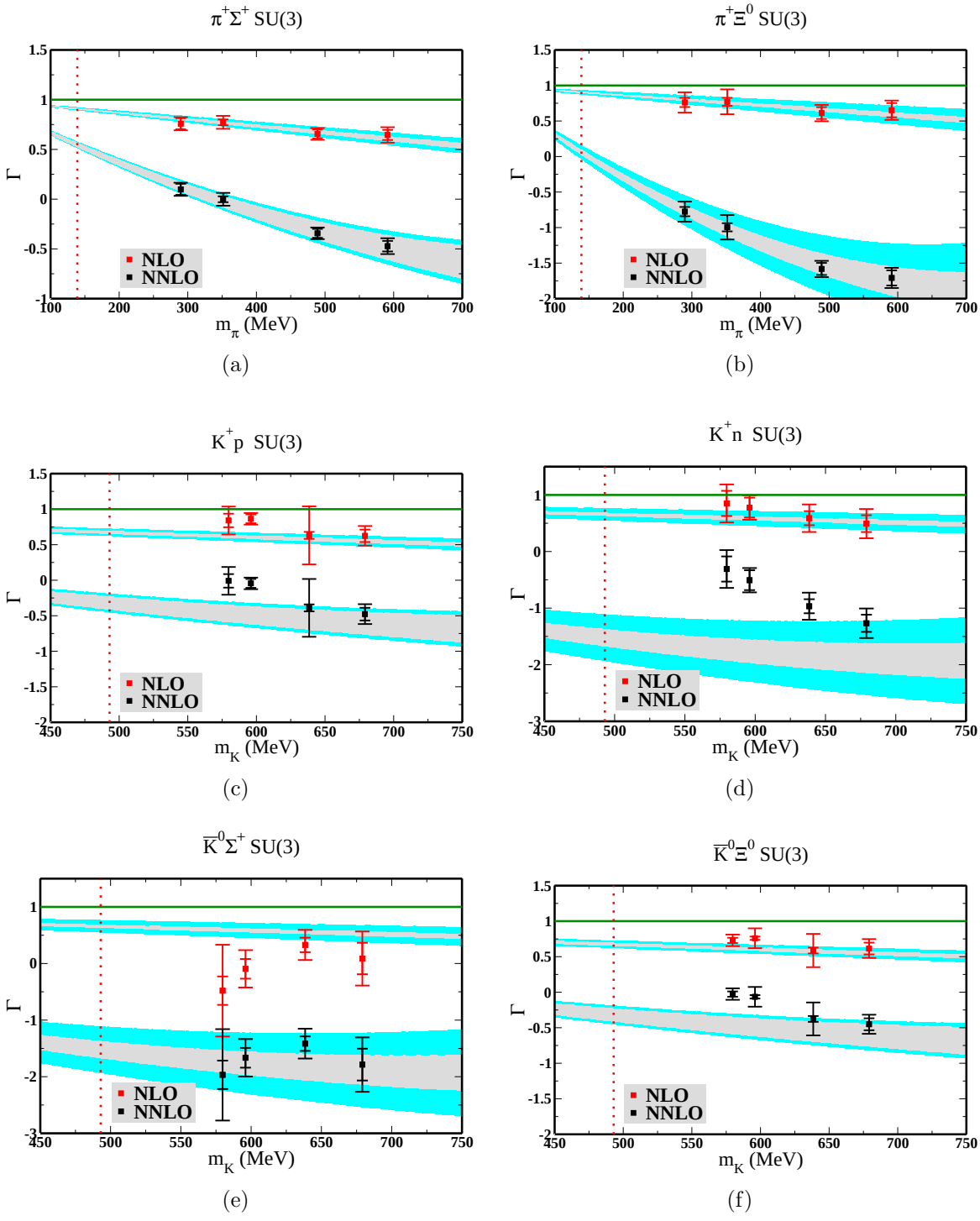


FIG. 5: Plots of $\Gamma_{NLO}$ and $\Gamma_{NNLO}$ versus the Goldstone masses. The line at $\Gamma = 1$ is the leading order curve, and dotted line is the physical meson mass. The innermost error bar is the statistical error and the outermost error bar is the statistical and systematic error added in quadrature. The inner and outer filled bands correspond to the statistical and systematic error, respectively, of the fits to the LECs at NLO and NNLO using $\pi^+\Sigma^+$, and $\pi^+\Xi^0$ *only*, for the SU(3) case.

| Quantity | LO (fm) | NLO fit (fm) | NLO (NNLO fit) (fm) | NNLO (NNLO fit) (fm) |
|---|---|---|---|---|
| $a_{\pi\Sigma}$ | -0.2294 | -0.208(01)(03) | -0.117(06)(08) | -0.197(06)(08) |
| $a_{\pi\Xi}$ | -0.1158 | -0.105(01)(04) | 0.004(05)(11) | -0.096(05)(12) |
| $a_{Kp}$ | -0.3971 | -0.311(18)(44) | 0.292(35)(48) | -0.154(51)(63) |
| $a_{Kn}$ | -0.1986 | -0.143(10)(27) | 0.531(28)(68) | 0.128(42)(87) |
| $a_{K\Sigma}$ | -0.2143 | -0.050(33)(60) | 0.573(30)(73) | 0.062(45)(94) |
| $a_{K\Xi}$ | -0.4406 | -0.331(12)(31) | 0.324(39)(54) | -0.127(57)(70) |

TABLE V: $SU(3)$ extrapolated scattering lengths using the LECs from Table IV. The first error in parentheses is statistical, and the second is the statistical and systematic error added in quadrature.

and two-flavor theories is described in detail in Ref. [17]. We make use of the formulation of the $\pi\Sigma$ and $\pi\Xi$ T-matrices from [17] to perform the two-flavor chiral extrapolations for $a_{\pi^+\Sigma^+}$, and $a_{\pi^+\Xi^0}$. As pointed out in Ref. [17], there are two representations of the pion-hyperon scattering lengths that are equivalent up to omitted higher orders in the chiral expansion; one contains a chiral logarithm, and the other is purely a polynomial in $m_\pi$. Using both forms provides a useful check on the systematics of the chiral extrapolation.

### A. Scattering Length Formulas I

To $\mathcal{O}(m_\pi^3)$ in the two-flavor chiral expansion, $a_{\pi^+\Sigma^+}$ and $a_{\pi^+\Xi^0}$ are given by [17]:

$$a_{\pi^+\Sigma^+} = \frac{1}{4\pi}\frac{m_\Sigma}{m_\pi + m_\Sigma}\left[ -\frac{2m_\pi}{f_\pi^2} + \frac{2m_\pi^2}{f_\pi^2}\mathrm{C}_{\pi^+\Sigma^+} + \frac{m_\pi^3}{\pi^2 f_\pi^4}\log\frac{m_\pi}{\mu} + \frac{2m_\pi^3}{f_\pi^2}h_{\pi^+\Sigma^+}(\mu)\right] \tag{36}$$

$$a_{\pi^+\Xi^0} = \frac{1}{4\pi}\frac{m_\Xi}{m_\pi + m_\Xi}\left[ -\frac{m_\pi}{f_\pi^2} + \frac{m_\pi^2}{f_\pi^2}\mathrm{C}_{\pi^+\Xi^0} + \frac{m_\pi^3}{2\pi^2 f_\pi^4}\log\frac{m_\pi}{\mu} + \frac{m_\pi^3}{f_\pi^2}h_{\pi^+\Xi^0}(\mu)\right] , \tag{37}$$

where the explicit forms —in terms of Lagrangian parameters— of the LECs $\mathrm{C}_{\pi^+\Sigma^+}$, $h_{\pi^+\Sigma^+}$, $\mathrm{C}_{\pi^+\Xi^0}$ and $h_{\pi^+\Xi^0}$ are given in Ref. [17]. As in the three flavor case, the mixed-action modification to the $SU(2)$ scattering length formula would begin with corrections to the $m_\pi^3\ln(m_\pi)$ terms, with the mixed valence-sea pions having the known additive mass shift [61]. We again choose $\mu = \Lambda_\chi = 4\pi f_\pi$ and evaluate $f_\pi$ at its lattice physical value. In analogy with the three-flavor case, here we define

$$\Gamma_{LO} \equiv 1 \ ; \tag{38}$$

$$\Gamma_{NLO} \equiv 1 - C_{\pi^+B} m_\pi \ ; \tag{39}$$

$$\Gamma_{NNLO} \equiv 1 - C_{\pi^+B} m_\pi - h_{\pi^+B}(\Lambda_\chi) m_\pi^2 \ , \tag{40}$$

where $B$ is either $\Sigma^+$ or $\Xi^0$. In figure 6 we give plots of $\Gamma_{NLO}$ and $\Gamma_{NNLO}$ versus the Goldstone masses for the two-flavor case. Clearly the deviations of $\Gamma$ from unity are consistent with a

| | NLO fit | NNLO fit |
|---|---|---|
| $C_{\pi^+\Sigma^+}$ | 0.66(04)(11) GeV$^{-1}$ | 1.98(17)(24) GeV$^{-1}$ |
| $C_{\pi^+\Xi^0}$ | 0.69(06)(22) GeV$^{-1}$ | 2.01(24)(68) GeV$^{-1}$ |
| $h_{\pi^+\Sigma^+}$ | - | -0.65(36)(40) GeV$^{-2}$ |
| $h_{\pi^+\Xi^0}$ | - | -0.6(0.5)(1.1) GeV$^{-2}$ |

TABLE VI: $SU(2)$ LECs fit from each process at NLO and at NNLO. The first error in parentheses is statistical, and the second is the statistical and systematic error added in quadrature.

| Quantity | LO (fm) | NLO (fm) | NLO (NNLO fit) (fm) | NNLO (fm) |
|---|---|---|---|---|
| $a_{\pi\Sigma}$ | -0.2294 | -0.208(01)(03) | -0.166(05)(08) | -0.197(06)(08) |
| $a_{\pi\Xi}$ | -0.1158 | -0.105(01)(04) | -0.083(04)(11) | -0.098(05)(12) |

TABLE VII: $SU(2)$ extrapolated scattering lengths using the LECs from Table VI. The first error in parentheses is statistical, and the second is the statistical and systematic error added in quadrature.

perturbative expansion at both NLO and NNLO. Notice that the loop corrections are much smaller at the scale $\Lambda_\chi$ than in the three-flavor case. The fit LECs are given in table VI and indeed all extracted LECs are of natural size. The extrapolated $\pi^+\Sigma^+$ and $\pi^+\Xi^0$ scattering lengths are given in table VII. The results are consistent with what was found in the three-favor extrapolation. The NLO and NNLO LECs are highly correlated in the NNLO fit. Figure 8 shows the 68% and 95% confidence interval error ellipses in the $h$-C plane for both $\pi^+\Sigma^+$ and $\pi^+\Xi^0$. Exploring the full 95% confidence interval error ellipse in the $h$-C plane yields

$$a_{\pi^+\Sigma^+} = -0.197 \pm 0.017 \text{ fm} ; \quad (41)$$

$$a_{\pi^+\Xi^0} = -0.098 \pm 0.017 \text{ fm} . \quad (42)$$

These are the numbers that we quote as our best determinations of the pion-hyperon scattering lengths.

### B. Scattering Length Formulas II

Ref. [17] makes the interesting observation that replacing $f_\pi$ with its chiral limit value, $f$, yields:

$$a_{\pi^+\Sigma^+} = \frac{1}{2\pi}\frac{m_\Sigma}{m_\pi + m_\Sigma}\left[ -\frac{m_\pi}{f^2} + \frac{m_\pi^2}{f^2}\mathrm{C}_{\pi^+\Sigma^+} + \frac{m_\pi^3}{f^2}h'_{\pi^+\Sigma^+}\right], \qquad h'_{\pi^+\Sigma^+} = \frac{4}{f^2}\ell_4^r + h_{\pi^+\Sigma^+} ; \quad (43)$$

$$a_{\pi^+\Xi^0} = \frac{1}{4\pi}\frac{m_\Xi}{m_\pi + m_\Xi}\left[ -\frac{m_\pi}{f^2} + \frac{m_\pi^2}{f^2}\mathrm{C}_{\pi^+\Xi^0} + \frac{m_\pi^3}{f^2}h'_{\pi^+\Xi^0}\right], \qquad h'_{\pi^+\Xi^0} = \frac{4}{f^2}\ell_4^r + h_{\pi^+\Xi^0} , \quad (44)$$

| | NLO fit | NNLO fit |
|---|---|---|
| $C_{\pi^+\Sigma^+}$ | 1.28(09)(11) GeV$^{-1}$ | 1.90(10)(17) GeV$^{-1}$ |
| $C_{\pi^+\Xi^0}$ | 1.84(23)(25) GeV$^{-1}$ | 1.93(12)(48) GeV$^{-1}$ |
| $h'_{\pi^+\Sigma^+}$ | - | -1.33(21)(26) GeV$^{-2}$ |
| $h'_{\pi^+\Xi^0}$ | - | -1.36(27)(75) GeV$^{-2}$ |

TABLE VIII: $SU(2)$ LECs fit from each process at NLO and at NNLO. The first error in parentheses is statistical, and the second is the statistical and systematic error added in quadrature.

| Quantity | LO (fm) | NLO (fm) | NLO (NNLO fit) (fm) | NNLO (fm) |
|---|---|---|---|---|
| $a_{\pi\Sigma}$ | -0.2294 | -0.212(03)(04) | -0.190(04)(06) | -0.197(04)(09) |
| $a_{\pi\Xi}$ | -0.1158 | -0.106(04)(05) | -0.095(02)(09) | -0.102(02)(09) |

TABLE IX: $SU(2)$ extrapolated scattering lengths using the LECs from Table VIII. The first error in parentheses is statistical, and the second is the statistical and systematic error added in quadrature.

where $\ell_4^r$ is the LEC which governs the pion mass dependence of $f_\pi$ [63]. Note that the chiral logs have canceled and therefore in this form, valid to order $m_\pi^3$ in the chiral expansion, the scattering lengths have a simple polynomial dependence on $m_\pi$. Taking the standard value $f = 122.9$ MeV [17, 63] and refitting the LECs yields the results tabulated in table VIII. The extrapolated $\pi^+\Sigma^+$ and $\pi^+\Xi^0$ scattering lengths are given in table IX. These results are clearly consistent with what was found in the two-flavor extrapolation with the chiral logarithm explicit. Figure 9 shows the 68% and 95% confidence interval error ellipses in the $h$-C plane for both $\pi^+\Sigma^+$ and $\pi^+\Xi^0$. Exploring the full 95% confidence interval error ellipse in the $h$-C plane yields

$$a_{\pi^+\Sigma^+} = -0.197 \pm 0.011 \text{ fm} ; \tag{45}$$

$$a_{\pi^+\Xi^0} = -0.102 \pm 0.004 \text{ fm} . \tag{46}$$

Comparison of these determinations with those of eq. (42) give an estimate of the systematic error due to truncation of the chiral expansion at order $m_\pi^3$. We have also "pruned" the data; that is, we have redone all fits omitting the heaviest mass ensemble. While this procedure inflates the errors, we see very little shift in the central values.

In order to plot the scattering length as a function of $m_\pi$, we define

$$\overline{a}_{\pi^+\Sigma^+} = a_{\pi^+\Sigma^+}\left(\frac{m_\pi + m_\Sigma}{m_\Sigma}\right) = \frac{1}{2\pi}\left(-\frac{m_\pi}{f^2} + \frac{m_\pi^2}{f^2}\mathrm{C}_{\pi^+\Sigma^+} + \frac{m_\pi^3}{f^2}h'_{\pi^+\Sigma^+}\right) ; \tag{47}$$

$$\overline{a}_{\pi^+\Xi^0} = a_{\pi^+\Xi^0}\left(\frac{m_\pi + m_\Xi}{m_\Xi}\right) = \frac{1}{4\pi}\left(-\frac{m_\pi}{f^2} + \frac{m_\pi^2}{f^2}\mathrm{C}_{\pi^+\Xi^0} + \frac{m_\pi^3}{f^2}h'_{\pi^+\Xi^0}\right) . \tag{48}$$

In Figure 7 we plot the scattering lengths versus the pion mass. The shaded bands in these plots correspond to the standard error in the determination of the LECs, as given in table VIII.

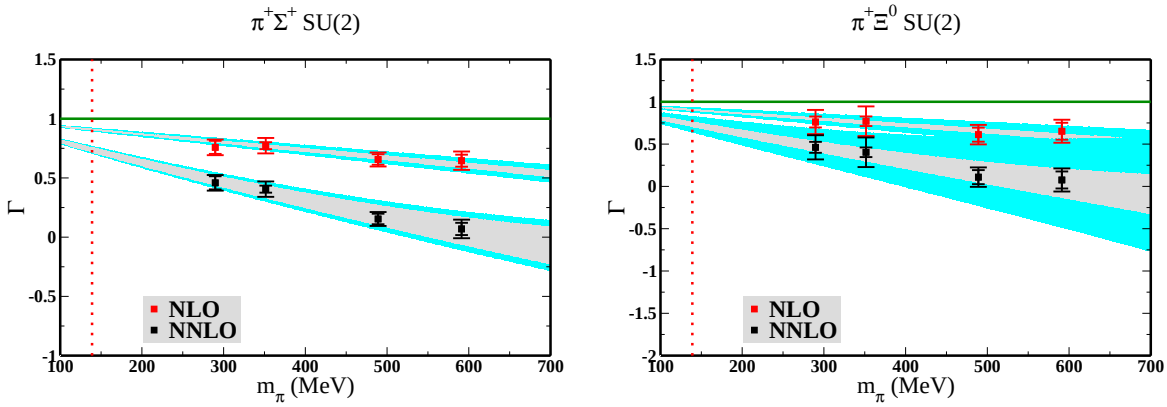


FIG. 6: $\Gamma_{NLO}$, $\Gamma_{NNLO}$ plots for the $\pi^+\Sigma^+$, and $\pi^+\Xi^0$ processes as a function of the pion mass. The line at $\Gamma = 1$ is the leading order curve, and the dotted line is the physical pion mass. The innermost error bar is the statistical error and the outermost error bar is the statistical and systematic error added in quadrature. The inner and outer filled bands correspond to the statistical and systematic error, respectively, of the fits to the LECs at NLO and NNLO using $\pi^+\Sigma^+$, and $\pi^+\Xi^0$ for the SU(2) case.

Additional systematic uncertainties arising from the specific lattice formulation that we employ are discussed in detail in Ref. [1], and are expected to be well encompassed by our error bars. As discussed in section III, there is a systematic error in extracting the scattering length from the phase shift. We find that range corrections affect the scattering length at the 5% level for $\pi^+\Sigma^+$, and at the 1% level for $\pi^+\Xi^0$. Finally, we reiterate that there are unquantified systematic errors due to finite-volume and lattice-spacing effects, however these uncertainties are likely encompassed by our quoted errors.

## VII. CONCLUSIONS

In this paper we have presented the first fully-dynamical lattice QCD calculation of meson-baryon scattering. While the phenomenologically most-interesting case of pion-nucleon scattering involves annihilation diagrams and therefore requires more resources than we currently have available, we have calculated the ground-state energies of $\pi^+\Sigma^+$, $\pi^+\Xi^0$, $K^+p$, $K^+n$, $\overline{K}^0\Sigma^+$, and $\overline{K}^0\Xi^0$, which involve no annihilation diagrams.

An analysis of the scattering lengths of these two-body systems using HB$\chi$PT has led us to conclude that the three-flavor chiral expansion does not converge over the range of light quark masses that we investigate. While the kaon-baryon scattering lengths appear perturbative at NLO, the large kaon loops destroy convergence at NNLO. Therefore, we do not quote values for the kaon-baryon scattering lengths at the physical point. On the other hand, the $\pi^+\Sigma^+$ and $\pi^+\Xi^0$ scattering lengths appear to have a well-controlled chiral expansion in two-flavor HB$\chi$PT. Our results, $a_{\pi^+\Sigma^+} = -0.197 \pm 0.017$ fm, and $a_{\pi^+\Xi^0} = -0.098 \pm 0.017$ fm, deviate from the LO (current algebra) predictions at the one- and two-sigma level, respectively. We look forward to confirmation of these predictions from other lattice QCD calculations and possibly from future experiments.

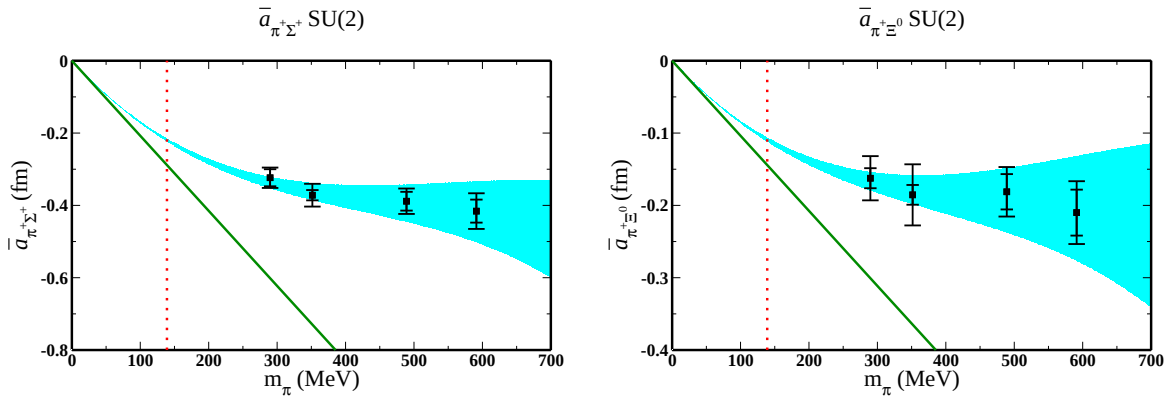


FIG. 7: $\bar{a}$ plots for the $\pi^+\Sigma^+$, and $\pi^+\Xi^0$ processes as a function of the pion mass. The dark, green line is the leading order curve, and the red, dotted line is the physical pion mass. The innermost error bar is the statistical error and the outermost error bar is the statistical and systematic error added in quadrature. The filled bands are the fits to the LECs in the SU(2) case at NNLO as in eqs. (47), and (48).

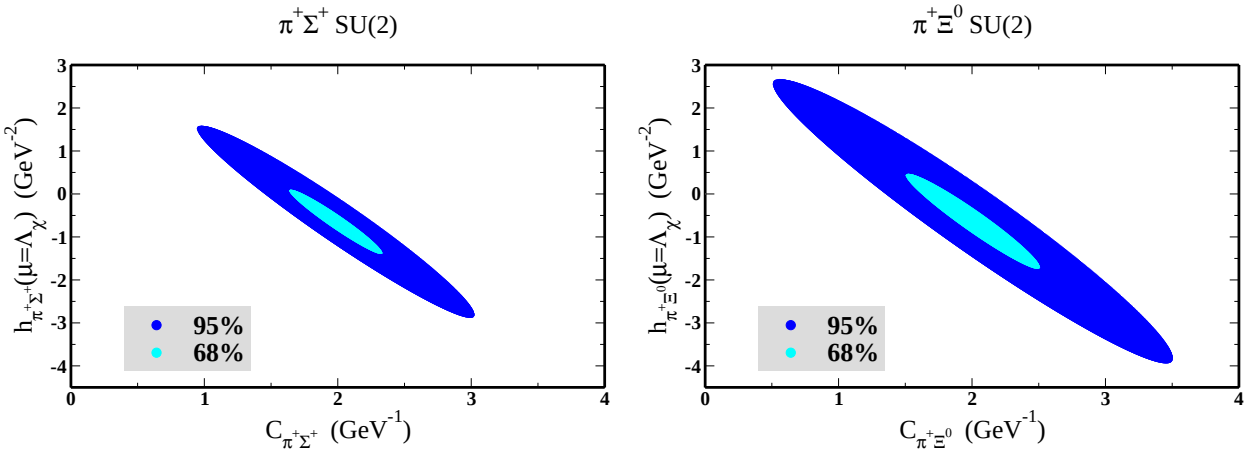


FIG. 8: The 68% (light) and 95% (dark) confidence interval error ellipses for fits for the $\pi^+\Sigma^+$ (left), and $\pi^+\Xi^0$ (right) processes using eqs. (36) and (37).

The HB$\chi$PT analyses performed in this work lead to a general conclusion about convergence in the three-flavor chiral expansion. As the pion masses considered in the lattice calculation are comparable to the physical kaon mass, the distinct convergence patterns of the two- three-flavor chiral expansions found in this work are suggestive that the breakdown of the three-flavor chiral is not due to the relative largeness of the strange-quark mass as compared to the light quark masses, but rather due to some other enhancement in the coefficients of the loop contributions, possibly related to a scaling with powers of $n_f$, the number of flavors.

While in this paper we have not considered the lowest-lying baryon decuplet, one interesting process for future study is the $\pi^-\Omega^-$ system. It does not involve disconnected diagrams

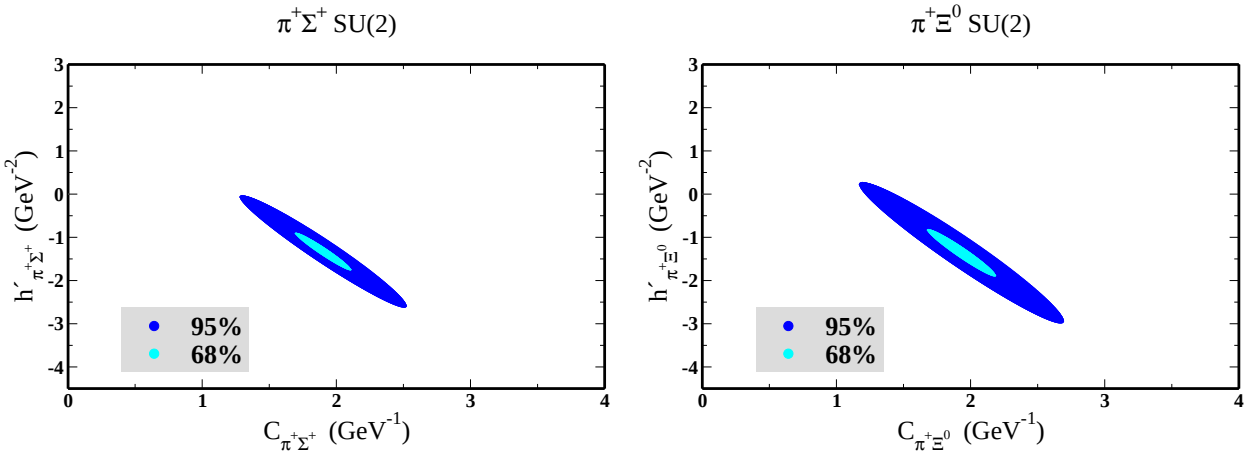


FIG. 9: The 68% (light) and 95% (dark) confidence interval error ellipses for fits for the $\pi^+\Sigma^+$ (left), and $\pi^+\Xi^0$ (right) processes using eqs. (43) and (44).

since the pions have no valence quarks with the same flavor as the $\Omega^-$ constituents. It has been argued that there is a bound state [64] in this channel and therefore it would be of interest to determine whether this state appears bound on the lattice at the available quark masses.

## VIII. ACKNOWLEDGMENTS

We thank M.J. Savage for contributing to the production of lattice data used in this work and for extensive discussions and comments on the manuscript. We also thank U.G. Meißner for useful discussions and R. Edwards and B. Joo for help with the QDP++/Chroma programming environment [65] with which the calculations discussed here were performed. The computations for this work were performed at Jefferson Lab, Fermilab, Lawrence Livermore National Laboratory, National Center for Supercomputing Applications, NERSC, Centro Nacional de Supercomputación (Barcelona, Spain) and the Institute for Nuclear Theory. The work of WD and KO was supported in part by the U.S. Dept. of Energy contract No. DE-AC05-06OR23177 (JSA) and by the Jeffress Memorial Trust, grant J-813, DOE OJI grant DE-FG02-07ER41527 and DOE grant DE-FG02-04ER41302. The work of SRB and AT was supported in part by the National Science Foundation CAREER grant No. PHY-0645570. Part of this work was performed under the auspices of the US DOE by the University of California, Lawrence Livermore National Laboratory under Contract No. W-7405-Eng-48. The work of AP was partly supported by the EU contract FLAVIAnet MRTN-CT-2006-035482, by the contract FIS2005-03142 from MEC (Spain) and FEDER and by the Generalitat de Catalunya contract 2005SGR-00343.
Prepared by LLNL under Contract DE-AC52-07NA27344.

[1] S. R. Beane, T. C. Luu, K. Orginos, A. Parreño, M. J. Savage, A. Torok and A. Walker-Loud, Phys. Rev. D **77**, 014505 (2008) [arXiv:0706.3026 [hep-lat]].

[2] S. R. Beane, P. F. Bedaque, T. C. Luu, K. Orginos, E. Pallante, A. Parreño and M. J. Savage, Phys. Rev. D **74**, 114503 (2006) [arXiv:hep-lat/0607036].

[3] S. R. Beane, T. C. Luu, K. Orginos, A. Parreño, M. J. Savage, A. Torok and A. Walker-Loud [NPLQCD Collaboration], Phys. Rev. D **77**, 094507 (2008) [arXiv:0709.1169 [hep-lat]].
[4] S. R. Beane, W. Detmold, T. C. Luu, K. Orginos, M. J. Savage and A. Torok, Phys. Rev. Lett. **100**, 082004 (2008) [arXiv:0710.1827 [hep-lat]].
[5] W. Detmold, M. J. Savage, A. Torok, S. R. Beane, T. C. Luu, K. Orginos and A. Parreno, Phys. Rev. D **78**, 014507 (2008) [arXiv:0803.2728 [hep-lat]].
[6] For a recent review, see V. Bernard, Prog. Part. Nucl. Phys. **60**, 82 (2008) [arXiv:0706.0312 [hep-ph]].
[7] S. R. Beane, P. F. Bedaque, K. Orginos and M. J. Savage, Phys. Rev. Lett. **97**, 012001 (2006) [arXiv:hep-lat/0602010].
[8] S. R. Beane, P. F. Bedaque, T. C. Luu, K. Orginos, E. Pallante, A. Parreño and M. J. Savage [NPLQCD Collaboration], Nucl. Phys. A **794**, 62 (2007) [arXiv:hep-lat/0612026].
[9] S. R. Beane *et al.*, arXiv:0903.2990 [hep-lat].
[10] G. P. Lepage, "The Analysis Of Algorithms For Lattice Field Theory," Invited lectures given at TASI'89 Summer School, Boulder, CO, Jun 4-30, 1989.
[11] D. B. Kaplan, M. J. Savage and M. B. Wise, Nucl. Phys. B **534**, 329 (1998) [arXiv:nucl-th/9802075].
[12] See, for instance, R. Babich, R. Brower, M. Clark, G. Fleming, J. Osborn and C. Rebbi, PoS **LATTICE2008**, 160 (2008) [arXiv:0901.4569 [hep-lat]].
[13] E. E. Jenkins and A. V. Manohar, "Baryon chiral perturbation theory using a heavy fermion Lagrangian," Phys. Lett. B **255**, 558 (1991).
[14] Y. R. Liu and S. L. Zhu, Phys. Rev. D **75**, 034003 (2007) [arXiv:hep-ph/0607100].
[15] Y. R. Liu and S. L. Zhu, Eur. Phys. J. C **52**, 177 (2007) [arXiv:hep-ph/0702246].
[16] N. Kaiser, Phys. Rev. C **64**, 045204 (2001) [Erratum-ibid. C **73**, 069902 (2006)] [arXiv:nucl-th/0107006].
[17] M. Mai, P. C. Bruns, B. Kubis and U. G. Meißner, arXiv:0905.2810 [hep-ph].
[18] D. B. Kaplan and A. E. Nelson, preprint HUTP-86/A023; Phys. Lett. B **175** (1986) 57; Phys. Lett. B **192**, 193 (1987); Nucl. Phys. A **479**, 273 (1988); Nucl. Phys. A **479**, 285 (1988);
[19] M. Lu, M. B. Wise and M. J. Savage, Phys. Lett. B **337**, 133 (1994) [arXiv:hep-ph/9407260].
[20] H. C. Schroder *et al.*, Phys. Lett. B **469**, 25 (1999).
[21] H. C. Schroder *et al.*, Eur. Phys. J. C **21**, 473 (2001).
[22] A. D. Martin, Nucl. Phys. B **179**, 33 (1981).
[23] M. Fukugita, Y. Kuramashi, M. Okawa, H. Mino and A. Ukawa, Phys. Rev. D **52**, 3003 (1995) [arXiv:hep-lat/9501024].
[24] G. w. Meng, C. Miao, X. n. Du and C. Liu, Int. J. Mod. Phys. A **19**, 4401 (2004) [arXiv:hep-lat/0309048].
[25] S. Weinberg, Phys. Rev. Lett. **17**, 616 (1966).
[26] B. C. Tiburzi, Phys. Rev. D **72**, 094501 (2005) [arXiv:hep-lat/0508019].
[27] J. W. Chen, D. O'Connell and A. Walker-Loud, JHEP **0904**, 090 (2009) [arXiv:0706.0035 [hep-lat]].
[28] J. W. Chen, D. O'Connell, R. S. Van de Water and A. Walker-Loud, Phys. Rev. D **73**, 074510 (2006) [arXiv:hep-lat/0510024].
[29] J. W. Chen, D. O'Connell and A. Walker-Loud, Phys. Rev. D **75**, 054501 (2007) [arXiv:hep-lat/0611003].
[30] S. R. Beane, K. Orginos and M. J. Savage, Int. J. Mod. Phys. E **17**, 1157 (2008) [arXiv:0805.4629 [hep-lat]].

[31] K. Huang and C. N. Yang, Phys. Rev. **105**, 767 (1957); H. W. Hamber, E. Marinari, G. Parisi and C. Rebbi, Nucl. Phys. B **225**, 475 (1983); M. Lüscher, Commun. Math. Phys. **105**, 153 (1986); M. Lüscher, Nucl. Phys. B **354**, 531 (1991).
[32] S. R. Beane, P. F. Bedaque, A. Parreño and M. J. Savage, Phys. Lett. B **585**, 106 (2004) [arXiv:hep-lat/0312004].
[33] D. B. Kaplan, Phys. Lett. B **288**, 342 (1992) [arXiv:hep-lat/9206013].
[34] Y. Shamir, Phys. Lett. B **305**, 357 (1993) [arXiv:hep-lat/9212010].
[35] Y. Shamir, Nucl. Phys. B **406**, 90 (1993) [arXiv:hep-lat/9303005].
[36] V. Furman and Y. Shamir, Nucl. Phys. B **439**, 54 (1995) [arXiv:hep-lat/9405004].
[37] Y. Shamir, Phys. Rev. D **59**, 054506 (1999) [arXiv:hep-lat/9807012].
[38] K. Orginos, D. Toussaint and R. L. Sugar, Phys. Rev. D **60**, 054503 (1999).
[39] K. Orginos and D. Toussaint, Phys. Rev. D **59**, 014501 (1999).
[40] C. W. Bernard *et al.*, Phys. Rev. D **64**, 054506 (2001).
[41] A. Hasenfratz and F. Knechtli, Phys. Rev. D **64**, 034504 (2001).
[42] T. A. DeGrand, A. Hasenfratz and T. G. Kovacs, Phys. Rev. D **67**, 054501 (2003).
[43] T. A. DeGrand, Phys. Rev. D **69**, 014504 (2004).
[44] M. Creutz, arXiv:hep-lat/0603020.
[45] C. Bernard, Phys. Rev. D **73**, 114503 (2006) [arXiv:hep-lat/0603011].
[46] C. Bernard, M. Golterman, Y. Shamir and S. R. Sharpe, Phys. Lett. B **649**, 235 (2007) [arXiv:hep-lat/0603027].
[47] M. Creutz, Phys. Lett. B **649**, 241 (2007).
[48] C. Bernard, M. Golterman and Y. Shamir, Phys. Rev. D **73**, 114511 (2006) [arXiv:hep-lat/0604017].
[49] C. Bernard, M. Golterman and Y. Shamir, PoS **LAT2006**, 205 (2006) [arXiv:hep-lat/0610003].
[50] M. Creutz, Phys. Lett. B **649**, 230 (2007) [arXiv:hep-lat/0701018].
[51] M. Creutz, arXiv:0704.2016 [hep-lat].
[52] S. Dürr, C. Hoelbling and U. Wenger, Phys. Rev. D **70**, 094502 (2004).
[53] S. Dürr and C. Hoelbling, Phys. Rev. D **71**, 054501 (2005) [arXiv:hep-lat/0411022].
[54] S. Dürr and C. Hoelbling, Phys. Rev. D **74**, 014513 (2006) [arXiv:hep-lat/0604005].
[55] A. Hasenfratz and R. Hoffmann, Phys. Rev. D **74**, 014511 (2006) [arXiv:hep-lat/0604010].
[56] Y. Shamir, Phys. Rev. D **75**, 054503 (2007) [arXiv:hep-lat/0607007].
[57] S. R. Sharpe, PoS **LAT2006**, 022 (2006) [arXiv:hep-lat/0610094].
[58] G. Dahlquist and Å. Björck, *Numerical Methods*, 1st ed., Prentice-Hall, 1974.
[59] S. R. Beane *et al.*, arXiv:0905.0466 [hep-lat].
[60] S. R. Beane, P. F. Bedaque, K. Orginos and M. J. Savage [NPLQCD Collaboration], Phys. Rev. D **73**, 054503 (2006) [arXiv:hep-lat/0506013].
[61] K. Orginos and A. Walker-Loud, Phys. Rev. D **77**, 094505 (2008) [arXiv:0705.0572 [hep-lat]].
[62] H. W. Lin and K. Orginos, Phys. Rev. D **79**, 034507 (2009) [arXiv:0712.1214 [hep-lat]].
[63] G. Colangelo, J. Gasser and H. Leutwyler, Nucl. Phys. B **603**, 125 (2001) [arXiv:hep-ph/0103088].
[64] W. L. Wang, F. Huang, Z. Y. Zhang, Y. W. Yu and F. Liu, Eur. Phys. J. A **32**, 293 (2007) [arXiv:nucl-th/0612007].
[65] R. G. Edwards and B. Joo [SciDAC Collaboration and LHPC Collaboration and UKQCD Collaboration], Nucl. Phys. Proc. Suppl. **140**, 832 (2005) [arXiv:hep-lat/0409003].